Journal of Applied Physics ARTICLE scitation.org/journal/jap

Critical thickness of hexagonal GaBN/BN heterostructures

Cite as: J. Appl. Phys. **125**, 205703 (2019); doi: 10.1063/1.5098796
Submitted: 3 April 2019 · Accepted: 5 May 2019 ·
Published Online: 24 May 2019

View Online Export Citation CrossMark

Q. W. Wang, J. Li, J. Y. Lin, and H. X. Jiang[a)]

AFFILIATIONS

Department of Electrical and Computer Engineering, Texas Tech University, Lubbock, Texas 79409, USA

[a)]**Email:** hx.jiang@ttu.edu

ABSTRACT

We report the growth of hexagonal boron gallium nitride alloys, h-$Ga_xB_{1-x}N$, on hexagonal boron nitride (h-BN) templates by metalorganic chemical vapor deposition and the observation of the critical thickness (L_C) phenomenon in the h-GaBN/BN heterostructure system. It was observed that $Ga_xB_{1-x}N$ alloys in a pure hexagonal phase can be obtained when the film thickness is below L_C. X-ray diffraction (XRD) θ–2θ measurement results revealed the formation of separate wurtzite (w)-GaN domains within the h-GaBN matrix when the film thickness is beyond L_C. XRD results were supported by photoluminescence spectroscopy which revealed the absence of the band edge emission of w-GaN near 3.4 eV in very thin layers, but an increase in the w-GaN band edge emission with an increase in the h-$Ga_xB_{1-x}N$ layer thickness beyond L_C. Despite the fact that layered structured materials generally possess a weak interlayer interaction, our results revealed that phase separation still occurs in layered h-$Ga_xB_{1-x}N$ alloys and the critical thickness depends on the Ga composition. The present study also provided insights into possible ways to synthesize layered GaBN/BN heterostructures and quantum wells in the pure hexagonal phase with tunable bandgaps and optical properties, which would open up many new applications.

INTRODUCTION

Hexagonal boron nitride (h-BN), as the only layer-structured material among the III-nitride semiconductors, has shown promising potential in optoelectronic applications, due to its exceptionally wide bandgap (>6.0 eV) and excellent optical properties.[1–5] The recent achievement of freestanding B-10 enriched h-BN epilayers of large thicknesses (>50 μm) has enabled the realization of thermal neutron detectors with a record high detection efficiency among solid-state detectors at 58%.[6,7] Today, 2D related materials and devices are also making extensive use of h-BN as a template, separation, and barrier layers.[8,9] BN[10] and p-BN/n-AlGaN heterostructures[11–13] have been explored for deep UV (DUV) device applications aimed to improve the p-type conduction in DUV emitters. For many device applications, the ability of bandgap engineering through alloying and heterojunction formation is highly desirable. Hexagonal (BN)C alloys have the potential to offer the bandgap tunability. It was shown that the optical properties of h-(BN)C alloys can be tuned within a small range in either the carbon-rich (less than 5% of BN) or BN-rich (less than 3% of C) side.[14,15] However, the h-(BN)C alloy material system faces the daunting challenge of phase separation arisen from the fundamental issue of differences in bond energies among B–C, B–N, and C–C bonds.[15,16]

An alternative way to achieve bandgap engineering in h-BN is to form alloys with GaN, namely, $Ga_xB_{1-x}N$ alloys. Despite the fact that the equilibrium phases of GaN and BN are wurtzite and hexagonal, respectively, we have previously demonstrated the synthesis of $Ga_xB_{1-x}N$ alloys in the hexagonal phase (or h-$Ga_xB_{1-x}N$) as well as h-$Ga_xB_{1-x}N$/h-BN quantum wells by metalorganic chemical vapor deposition (MOCVD).[17] It was observed that the use of the h-BN template is necessary to promote $Ga_xB_{1-x}N$ to crystallize into the hexagonal phase; however, only up to 7% of Ga composition can be incorporated into h-GaBN alloys deposited at a growth temperature of 1225 °C, most likely due to the effect of decomposition of GaN at this growth temperature. It is desirable to find ways to produce h-GaBN alloys offering an extended range of variation in the bandgap as well as in the optical and electrical properties. However, this would require a better understanding of the basic properties of h-$Ga_xB_{1-x}N$/h-BN heterostructures. One of the fundamental issues of heterostructure epitaxy is critical thickness (L_C). Here, we report the observation of critical thickness (L_C) phenomenon in layered h-$Ga_xB_{1-x}N$ alloys deposited on h-BN templates.

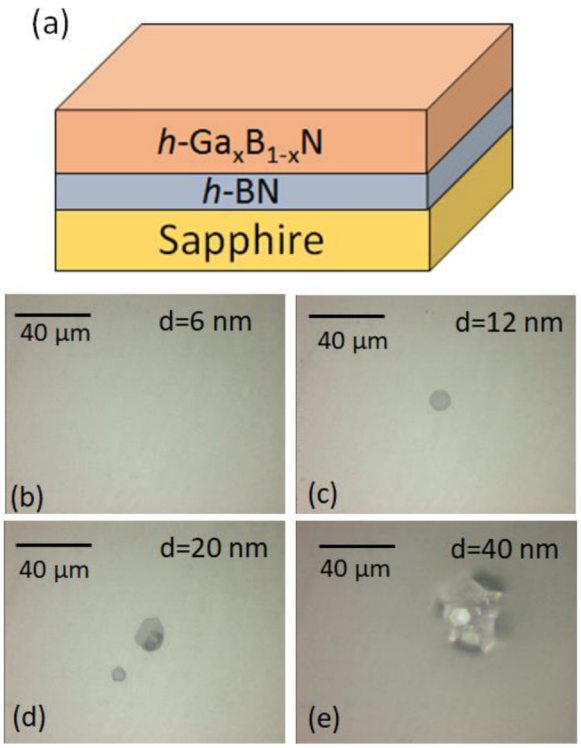

FIG. 1. (a) The schematic diagram of *h*-GaBN/BN heterostructure. Microscopy images of *h*-Ga$_x$B$_{1-x}$N alloys grown under a TMGa flow rate of R_{TMG} = 5 sccm with different thicknesses: (b) d = 6 nm, (c) d = 12 nm, (d) d = 20 nm, and (e) d = 40 nm.

It was observed that beyond L_C, the formation of wurtzite GaN domains inside *h*-Ga$_x$B$_{1-x}$N films tends to occur. Furthermore, it was observed that the critical thickness increases with a decrease of the Ga composition in *h*-Ga$_x$B$_{1-x}$N.

EXPERIMENTS

MOCVD was employed to synthesize *h*-Ga$_x$B$_{1-x}$N alloys. Prior to the growth of *h*-GaBN, a *h*-BN layer with 5 nm thickness was first deposited on the *c*-plane sapphire substrate at 1100 °C, followed by the growth of *h*-GaBN alloys at the same temperature. The growth temperature was reduced compared to 1225 °C in a previous reported work[17] with the aim to reduce the effect of GaN decomposition. The schematic diagram of the *h*-GaBN/BN heterostructure is shown in Fig. 1(a). Triethylboron (TEB), trimethylgallium (TMGa), and ammonia (NH_3) were used as precursors for B, Ga, and N, respectively, and hydrogen was used as a carrier gas. During the MOCVD growth, the TEB and NH_3 flow rates were kept constant. The Ga composition in *h*-GaBN alloys was controlled by varying the TMGa flow rate (R_{TMG}), which was later confirmed by X-ray photoelectron spectroscopy (XPS). Crystalline structure was determined by X-ray diffraction (XRD) measurements. Photoluminescence (PL) measurements were also used to monitor the emission properties of the grown layers. The PL system consists of an excimer laser operating at 193 nm and a portable spectrometer (Ocean Optics).

Two sets of *h*-GaBN samples with varying thicknesses were grown under R_{TMG} = 5 and 20 sccm. The *h*-GaBN layers with varying thicknesses (*d*) were prepared by varying the growth time. The profilometer measurement was used to determine the layer thickness. First, we scratched the sample's surface by using a

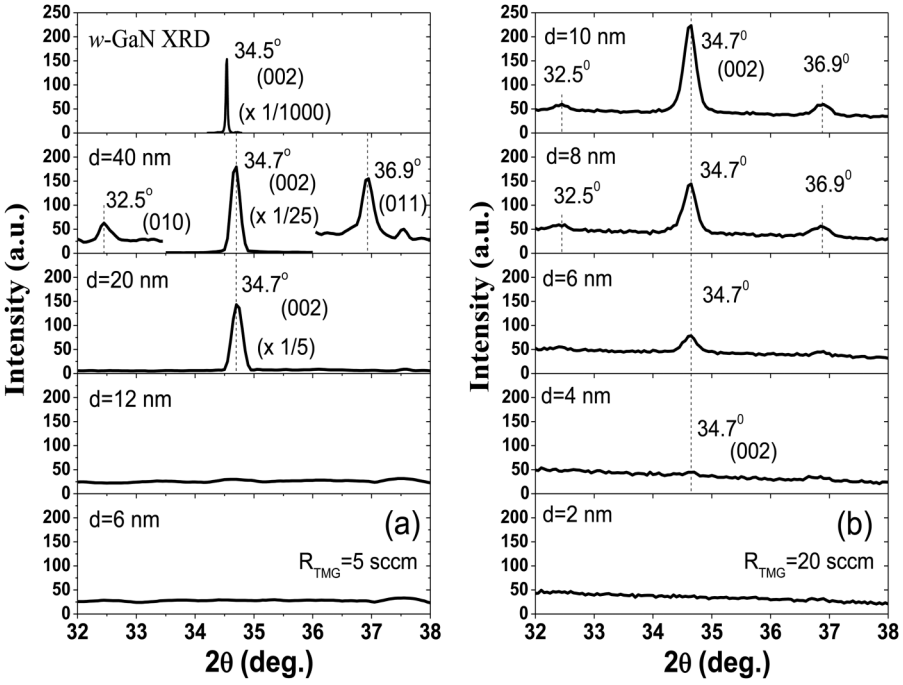

FIG. 2. XRD θ–2θ scans of *h*-GaBN/BN heterostructures samples of different layer thicknesses grown under (a) R_{TMG} = 5 sccm and (b) R_{TMG} = 20 sccm. As a reference, XRD θ–2θ scan of (002) peak for a wurtzite (w)-GaN epilayer is also shown at the top panel of (a).

tweezer. The scratch will cut through the *h*-BGaN/BN layer and stop at the sapphire surface. A profilometer was used to scan across this scratched line, and the depth probed is the total thickness of the *h*-BGaN/BN heterostructure. The thickness of *h*-BGaN layer was obtained by subtracting the *h*-BN layer thickness from the total thickness. The obtained thickness of *h*-BGaN alloys as described above was also consistent with estimation from the total growth time by knowing the growth rate from a thick layer.

RESULTS AND DISCUSSION

The microscopy images of the set of samples grown under $R_{TMG} = 5$ sccm are shown in Figs. 1(b)–1(e), and the results indicate that the 6 nm thick *h*-GaBN layer sample exhibits a very smooth surface. However, the formation of extra complex features with their sizes increasing with the layer thickness (d) is clearly observed in films with thicknesses greater than 12 nm. For the film with $d = 40$ nm, the extra feature becomes quite large with its dimension as large as 50 μm. Different colors and brightness exhibited by the extra feature in the microscopy images may reflect the presence of domains of different crystalline orientations.

To further understand the nature of this extra feature, XRD θ–2θ scans were employed to assess the crystalline structures of both sets of samples grown under (a) $R_{TMG} = 5$ sccm and (b) 20 sccm with different thicknesses, and the results are shown in Fig. 2, covering the spectral range of the wurtzite (w)-GaN (002) peak between 32° and 38°. XRD θ–2θ scan of an MOCVD grown w-GaN epilayer was included as a reference in the top panel of Fig. 2(a), exhibiting a w-GaN (002) peak at 34.5°. As shown in Fig. 2(a), for the set of samples grown with $R_{TMG} = 5$ sccm, no w-GaN peak was observed for $d = 6$ and 12 nm. However, the w-GaN (002) peak was clearly resolved at about 34.7° in thick layers with $d = 20$ nm and 40 nm. The shift in the (002) peak position from 34.5° for the w-GaN epilayer to 34.7° for w-GaN domains inside *h*-GaBN alloys is most likely due to the presence of strain in w-GaN domains. As d further increases to 40 nm, in addition to GaN (002) peak, other peaks corresponding to w-GaN (010) at 32.5° and GaN (011) at 36.9° were also observable. For the set of samples grown under $R_{TMG} = 20$ sccm, the w-GaN (002) peak was absent only in the sample with d = 2 nm and it starts to appear at $d = 4$ nm, as shown in Fig. 2(b). The (010) peak and the (011) peak of the w-GaN phase were also observed as d further increases to above 6 nm. XRD results seem to suggest that the extra feature seen in Fig. 1 is related to the formation of the w-GaN phase inside the *h*-GaBN matrix, and it is only observable when d is beyond 12 nm in samples grown under $R_{TMG} = 5$ sccm [Fig. 2(a)] and 2 nm in samples grown under $R_{TMG} = 20$ sccm [Fig. 2(b)].

In Fig. 3, we plot the w-GaN (002) XRD peak intensity vs *h*-GaBN alloy thickness, d, for (a) $R_{TMG} = 5$ sccm and (b) $R_{TMG} = 20$ sccm. The intensity of w-GaN (002) peak at 34.7° displays a power law dependence on d when d is beyond ~6 nm for $R_{TMG} = 5$ sccm and ~2 nm for $R_{TMG} = 20$ sccm. We believe that the results are indicative of a phase separation, meaning that w-GaN domains start to form inside layer-structured *h*-GaBN alloys when d is beyond a critical layer thickness (L_C). When *h*-GaBN film thickness is less than L_C, no phase separation occurs. To determine L_C quantitatively, the following relationship was used to describe

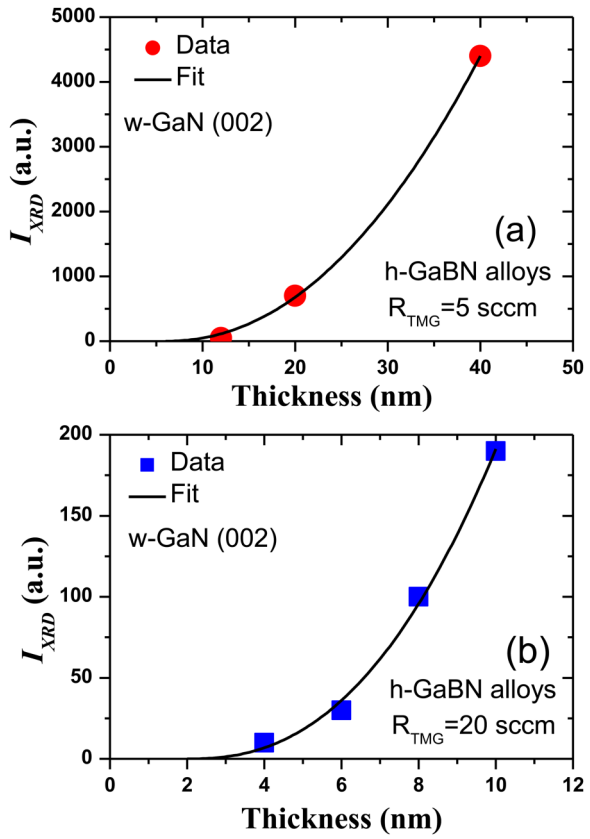

FIG. 3. The w-GaN XRD (002) peak intensity vs *h*-GaBN layer thickness d for samples grown under (a) $R_{TMG} = 5$ sccm and (b) $R_{TMG} = 20$ sccm. The solid curves are the least squares fits of data with Eq. (1).

the XRD w-GaN (002) peak intensity (I_{XRD}) vs layer thickness d:

$$I_{XRD}(d) = I_0(d - L_C)^n. \quad (1)$$

The least squares fit of data with Eq. (1) yielded values $I_0 = 3.0$ (1.5), $L_C = 6$ nm (2 nm), and $n = 2.1$ (2.4) for the set of samples grown with $R_{TMG} = 5$ (20) sccm. The results shown in Fig. 3 indicate that the critical thickness, L_C, depends on the Ga composition of *h*-GaBN alloys, as expected. The w-GaN (002) peak intensity increases with L_C following a power law dependence with an exponent n being very close to 2, which is probably related to the fact that *h*-GaBN films are two-dimensional (2D) in nature. The results suggest that the formation of w-GaN polycrystalline structures inside *h*-GaBN occurs when d is larger than L_C.

Room temperature PL spectra for these two sets of *h*-GaBN/BN heterostructure samples have been measured and are plotted in Fig. 4 for samples grown under (a) $R_{TMG} = 5$ sccm and (b) $R_{TMG} = 20$ sccm. The PL spectrum of the w-GaN epilayer is also included in the top panel of Fig. 4(a) as a reference, which exhibits a strong band edge emission line at 3.39 eV. For films grown under $R_{TMG} = 5$ sccm, the band edge emission line from

the wurtzite phase GaN is absent for the sample with $d = 6$ nm and a small peak near 3.34 eV starts to emerge for samples with $d > 12$ nm. In fact, this emission line at 3.34 eV becomes rather prominent in the sample with $d = 40$ nm. We believe that the 3.34 eV line is the band edge emission of w-GaN domains inside h-GaBN, which is redshifted with respect to 3.39 eV observed in w-GaN epilayers. This redshift is due to the same strain which also caused a small shift in the XRD (002) peak position of w-GaN domains in h-GaBN alloys with respect to that of the w-GaN epilayer shown in Fig. 2.

For the set of samples grown under $R_{TMG} = 20$ sccm, the emission line near 3.34 eV related to w-GaN domains was absent only in the sample with $d = 2$ nm and it starts to emerge in the sample with $d = 4$ nm and then further enhances with the layer thickness and becomes the dominant emission line in the sample with $d = 10$ nm. PL results for both sets of samples show that the emission line near 3.34 eV related to w-GaN domains increases with the h-GaBN thickness (d) when d is beyond L_C, which again suggest that a phase transition occurs at $d \sim L_C$ with $L_C \sim 6$ nm for samples grown under $R_{TMG} = 5$ sccm and $L_C \sim 2$ nm for samples grown under $R_{TMG} = 20$ sccm. Thus, the PL results collaborate well with XRD results. In addition to the band edge emission line of w-GaN domains in h-GaBN observed at 3.34 eV, a broad peak near 3.9 eV is believed to be associated with a shallow donor to deep acceptor (DAP) transition in h-GaBN alloys, as its spectral features and peak position are very close to a DAP transition in h-BN epilayers.[18]

The Ga composition x in h-$Ga_xB_{1-x}N$ alloys was determined by XPS. First, a survey spectrum was collected from a representative sample grown with $R_{TMG} = 20$ sccm. The B 1s, N 1s, Ga 3d, and C 1s peaks were all resolved in the survey spectrum shown in Fig. 5(a). The C 1s peak (284.8 eV) is due to surface contamination while transporting samples in the air, which was used as a reference. Then, each sample was sputtered with low energy (500 eV) Ar^+ ions for 30 s to remove C atoms on the surfaces. High resolution spectra were then obtained by employing high resolution scans. Corresponding transitions of B 1s at 190.4 eV, N 1s at 398.1 eV, and Ga 3d at 19.6 eV were observed and are shown in Figs. 5(b)–5(d), respectively. The measured average B, N, and Ga compositions in the sample with $d = 10$ nm grown under $R_{TMG} = 20$ sccm are 46.5%, 50.1%, and 3.4%, respectively, corresponding to h-$Ga_xB_{1-x}N$ alloys with $x = 0.068$. With the same procedure, we obtained a Ga composition of $x = 0.034$ in the h-$Ga_xB_{1-x}N$ alloy for the sample grown under $R_{TMG} = 5$ sccm.

Phase separation in ternary alloys $A_xB_{1-x}C$ is generally due to the internal elastic strain, caused by the lattice constants mismatch between two binary constituents AC and BC and the underlying epilayers template.[19] The origin of phase separation observed here in h-GaBN alloys differs from a ternary alloy of the same crystalline structure such as InGaN alloys. The stable phase of BN in our growth condition is hexagonal, while that of GaN is wurtzite. This implies that a phase transition will occur when Ga composition is above a critical value. Therefore, it is not a surprise to observe a phase transition in h-GaBN alloys. What is interesting, however, is the observation of the critical thickness in this layer-structured alloy system. It is well known that interlayer interaction is very weak in 2D materials. However, our results described here indicate that interlayer interaction is strong enough to give rise to a critical thickness for h-GaBN alloys, beyond which phase separation is to set in. The critical thickness (L_C) of a lattice mismatched heterostructure can be

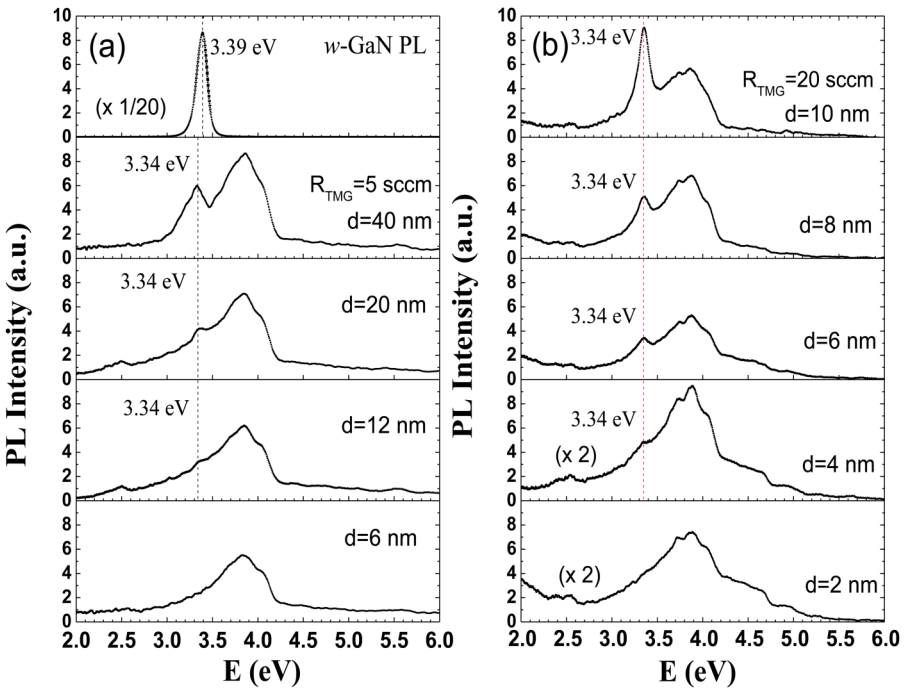

FIG. 4. Room temperature photoluminescence (PL) spectra of h-GaBN alloys of different layer thickness d for samples grown under (a) $R_{TMG} = 5$ sccm and (b) $R_{TMG} = 20$ sccm. For comparison, the PL spectrum of a GaN epilayer in the wurtzite phase (w-GaN) is presented in the top panel of Fig. 4(a).

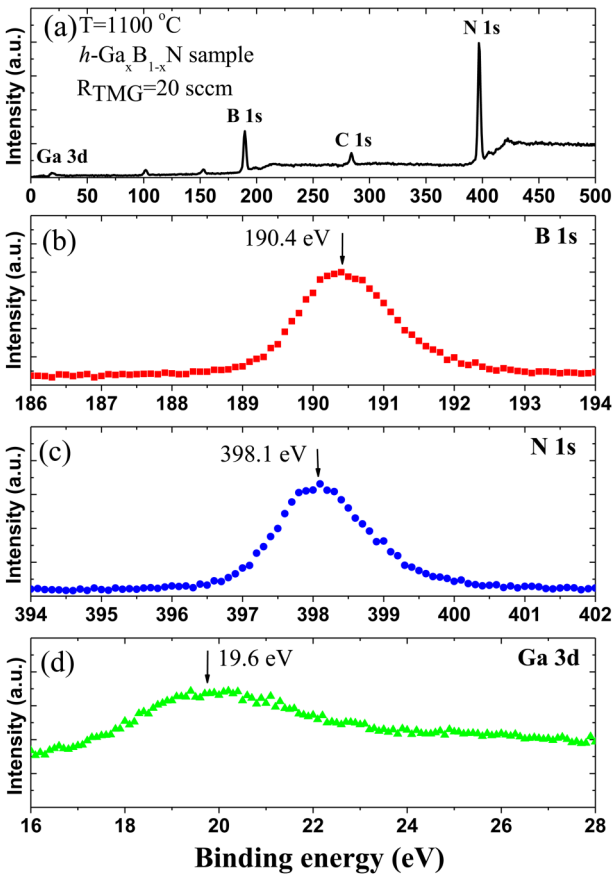

FIG. 5. X-ray photoelectron spectroscopy (XPS) spectra of an *h*-GaBN sample of $d = 10$ nm grown under $R_{TMG} = 20$ sccm. (a) Survey spectra. Narrow energy range spectra for peaks of (b) B 1s, (c) N 1s, and (d) Ga 3d.

calculated based on the strain energy[19,20] and can be further simplified to the following relation:[21]

$$L_C\ (\text{nm}) \cong 0.1\frac{a_s}{f}. \tag{2}$$

Here, a_s is the lattice constant of the underlying template (*h*-BN in our case) and f is the misfit between the subsequent epilayer (*h*-$Ga_xB_{1-x}N$ layer) and the underlying template layer, which is defined by

$$f = \frac{a_e - a_s}{a_s} = \frac{b}{a_s}x, \tag{3}$$

where a_e is the lattice constant of the *h*-$Ga_xB_{1-x}N$ layer, which is proportional to Ga composition, x. From Eqs. (2) and (3), we obtain a simple linear relationship between the critical thickness L_C and Ga composition x of *h*-GaBN alloys as

$$L_C\ (\text{nm}) = A \cdot \frac{1}{x}, \tag{4}$$

where A is a proportionality constant. In Fig. 6, we plot

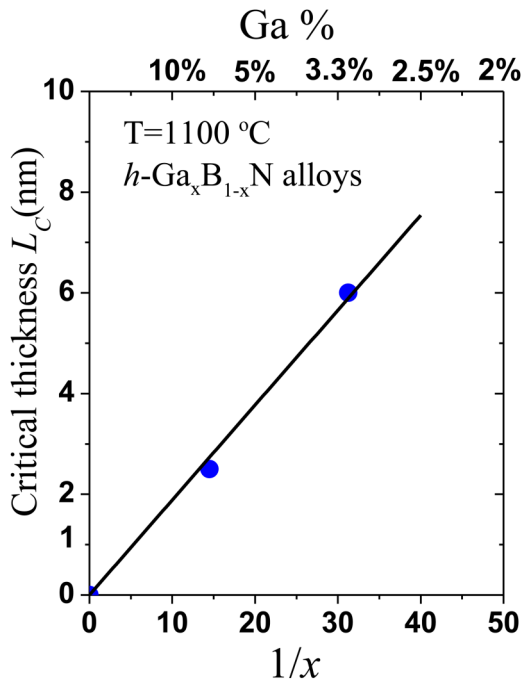

FIG. 6. Ga composition (x) dependence of the critical thickness (L_C) of *h*-$Ga_xB_{1-x}N$ alloys. Solid circles are experimental data and the solid line is the least squares fit of data with Eq. (4).

experimentally measured L_C for two different Ga composition x. Fitting of L_C vs $1/x$ in Fig. 6 provides a fitting parameter A = 0.19. The simplified theory of Eq. (2), which was developed for 3D materials, seems to be applicable to layered heterostructures. Figure 6 reveals that by further reducing the *h*-GaBN layer thickness, it is possible to increase the Ga composition in *h*-GaBN alloys without phase separation. For instance, in the extreme case with $L_C = 1$ monolayer = 0.33 nm, *h*-$Ga_xB_{1-x}N$ films with a Ga composition as high as $x = 0.5$ can be prepared without phase separation.

In summary, $Ga_xB_{1-x}N$ alloys in the hexagonal phase have been synthesized by MOCVD. A Ga composition dependent critical thickness L_C was observed in layered *h*-GaBN alloys. The dependence of L_C on the alloy composition can be described well by a simplified theory developed from 3D heterostructure materials. These results would further guide us on the development of layered *h*-GaBN/BN heterostructure and QWs. Directly imaging the structural evolution through measurements such as transmission electron microscopy may be possible and would be interesting. The observation of critical thickness in layered heterostructures also revealed new questions and provides new opportunities for fundamental understanding and many potential applications.

ACKNOWLEDGMENTS

This work is supported by U.S. Army Research Office (ARO) (No. W911NF-16-1-0268) and monitored by Dr. Michael Gerhold. H. X. Jiang and J. Y. Lin are grateful to the AT&T Foundation for the support of Ed Whitacre and Linda Whitacre endowed chairs.

REFERENCES

[1]Y. Kubota, K. Watanabe, O. Tsuda, and T. Taniguchi, Science **317**, 932 (2007).
[2]K. B. Arnaud, S. Lebègue, P. Rabiller, and M. Alouani, Phys. Rev. Lett. **96**, 026402 (2006).
[3]L. Wirtz, A. Marini, and A. Rubio, Phys. Rev. Lett. **96**, 126104 (2006).
[4]X. Z. Du, J. Li, J. Y. Lin, and H. X. Jiang, Appl. Phys. Lett. **108**, 052106 (2016).
[5]T. C. Doan, J. Li, J. Y. Lin, and H. X. Jiang, Appl. Phys. Lett. **109**, 122101 (2016).
[6]A. Maity, T. C. Doan, J. Li, J. Y. Lin, and H. X. Jiang, Appl. Phys. Lett. **109**, 072101 (2016).
[7]A. Maity, S. J. Grenadier, J. Li, J. Y. Lin, and H. X. Jiang, J. Appl. Phys. **123**, 044501 (2018).
[8]C. R. Dean, A. F. Young, I. Meric, C. Lee, L. Wang, S. Sorgenfrei, K. Watanabe, T. Taniguchi, P. Kim, K. L. Shepard, and J. Hone, Nat. Nanotechnol. **5**, 722 (2010).
[9]A. K. Geim and I. V. Grigorieva, Nature **499**, 419 (2013).
[10]K. Watanabe, T. Taniguchi, and H. Kanda, Nat. Mater. **3**, 404 (2004).
[11]R. Dahal, J. Li, S. Majety, B. N. Pantha, X. K. Cao, J. Y. Lin, and H. X. Jiang, Appl. Phys. Lett. **98**, 211110 (2011).
[12]S. Majety, J. Li, X. K. Cao, R. Dahal, B. N. Pantha, J. Y. Lin, and H. X. Jiang, Appl. Phys. Lett. **100**, 061121 (2012).
[13]D. A. Laleyan, S. Zhao, S. Y. Woo, H. N. Tran, H. B. Le, T. Szkopek, H. Guo, G. A. Botton, and Z. Mi, Nano Lett. **17**, 3738 (2017).
[14]M. R. Uddin, S. Majety, J. Li, J. Y. Lin, and H. X. Jiang, J. Appl. Phys. **115**, 093509 (2014).
[15]M. R. Uddin, J. Li, J. Y. Lin, and H. X. Jiang, J. Appl. Phys. **117**, 215703 (2015).
[16]K. Yuge, Phys. Rev. B **79**, 144109 (2009).
[17]Q. W. Wang, M. R. Uddin, X. Z. Du, J. Li, J. Y. Lin, and H. X. Jiang, Appl. Phys. Exp. **12**, 011002 (2019).
[18]X. Z. Du, J. Li, J. Y. Lin, and H. X. Jiang, Appl. Phys. Lett. **106**, 021110 (2015).
[19]S. Y. Karpov, MRS Internet J. Nitride Semicond. Res. **3**, e16 (1998).
[20]J. H. Van der Merwe, J. Appl. Phys. **34**, 123 (1962).
[21]R. People and J. C. Bean, Appl. Phys. Lett. **47**, 322 (1985).